Low-temperature static and dynamic behavior of the two-dimensional easy-axis Heisenberg model

M. E. Gouvêa, G. M. Wysin,* S. A. Leonel, A. S. T. Pires, T. Kamppeter,† and F. G. Mertens†
Departamento de Física, Instituto de Ciências Exatas, Universidade Federal de Minas Gerais, Belo Horizonte, CP 702, CEP 30123-970, MG, Brazil
(Received 15 May 1998; revised manuscript received 31 August 1998)

We apply the self-consistent harmonic approximation (SCHA) to study static and dynamic properties of the two-dimensional classical Heisenberg model with easy-axis anisotropy. The static properties obtained are magnetization and spin wave energy as functions of temperature, and the critical temperature as a function of the easy-axis anisotropy. We also calculate the dynamic correlation functions using the SCHA renormalized spin wave energy. Our analytical results, for both static properties and dynamic correlation functions, are compared to numerical simulation data combining cluster–Monte Carlo algorithms and spin dynamics. The comparison allows us to conclude that far below the transition temperature, where the SCHA is valid, spin waves are responsible for all relevant features observed in the numerical simulation data; topological excitations do not seem to contribute appreciably. For temperatures closer to the transition temperature, there are differences between the dynamic correlation functions from SCHA theory and spin dynamics; these may be due to the presence of domain walls and solitons. [S0163-1829(99)03809-6]

I. INTRODUCTION

Low-dimensional magnets have been extensively investigated by many theorists and experimentalists in the last three decades. More recently, the interest on the properties of two-dimensional (2D) Heisenberg magnets has been greatly revived since the discovery of high-T_c superconductivity: it is now well known[1] that the undoped, insulating La_2CuO_4 has a quasi-two-dimensional antiferromagnetic behavior. However, most quasi-two-dimensional magnetic real materials exhibit some kind of anisotropy: the anisotropic properties often arise not so much from an anisotropy in the interaction mechanism (which can be wholly isotropic) but from other sources, such as the presence of a crystal field that couples the spins to a certain direction in the crystal. Then, at least from a theoretical point of view, a large amount of magnetic materials fits (under certain circumstances like temperature range) into one of the two groups: easy-plane or easy-axis models. Easy-plane 2D magnets have deserved a lot of attention due to their possibility of showing the topological Kosterlitz-Thouless phase transition.[2] The interest devoted to easy-axis magnetic systems has been considerably smaller, specially concerning the study of its dynamical properties. It is our aim to address this topic in this paper.

It must be emphasized that, although we shall be concerned only with magnetic systems in this paper, many of the magnetic Hamiltonians also allow for an interpretation other than a magnetic one. Most physical problems concerning mutually interacting elements that form a spatial array can be mapped into a magnetic Hamiltonian by describing it within a pseudo spin formalism. The advantage of studying a general physical problem in its magnetic form is clearly that in magnetism several experimental techniques are available to study the fundamental properties of a system.[3]

The analysis of the general Ising-Heisenberg model is of interest because, from the experimental point of view, the presence of some degree of anisotropy in the interaction is to be expected in nearly all cases. In addition, recently there has been a growing interest in the study of topological excitations in the classical two-dimensional easy-axis model.[4] Having finite excitation energy, the population of topological objects should be quite small at low temperatures. Therefore, before taking into account the effect of topological excitations (solitons or similar objects) on the thermodynamics and dynamics of a system, we should consider the contribution of anisotropic spin waves. So we might ask: can spin waves explain experimental data or, in the absence of experiments, computer simulation data at low temperatures? This is the spirit and aim of this paper.

Here we consider the classical Heisenberg ferromagnet in two dimensions (2D) with easy-axis exchange anisotropy

$$H=-J\sum_{\mathbf{n},\mathbf{a}}\mathbf{S}_{\mathbf{n}}\cdot\mathbf{S}_{\mathbf{n}+\mathbf{a}}-K\sum_{\mathbf{n},\mathbf{a}}S^z_{\mathbf{n}}S^z_{\mathbf{n}+\mathbf{a}}, \tag{1}$$

where the summations run over all distinct couples of spin sites **n** and its nearest neighbors **a**. As the anisotropy parameter K ranges from 0 to ∞, we go from the isotropic Heisenberg model to an Ising *like* model in which the spins tend to be confined along the $\pm z$ direction. However, the resemblance to the Ising behavior can only hold for $T \ll K$: we find that, for Hamiltonian (1), $T_c \approx K$ for large K. This contrasts with $T_c \approx 2.27K$ for the 2D single-component Ising model.

In addition to the usual domain walls we expect that there can be localized solitonlike excitations that can connect a small circular domain of positive S^z to a surrounding region with negative S^z. A spatial ''width'' of these objects (bubbles or droplets) can be estimated as approximately $\sqrt{J/K}$. For intermediate values of $\sqrt{J/K}$, i.e., between a lattice constant and the system size, these excitations can be important on a finite discrete system. These objects can also have a topological charge or winding number of the spin field. There was some indication in earlier Monte Carlo

(MC) simulations[5] that they may play a role in the phase transition in this model; their density was found to increase strongly passing through the transition temperature. However, in a continuum static description they are found to be energetically unstable, according to the Derrick-Hobart theorem.[6] Thus it makes sense to investigate whether it is necessary to be aware of their presence in static and dynamic properties of this model, or whether a description based on anisotropic spin waves is sufficient.

To this end we study the low-temperature thermodynamics and dynamics of this model using a self-consistent harmonic approximation theory (SCHA) to treat spin waves. As is well known, the SCHA is a reasonable approximation to calculate the transition temperature and low-temperature ($T<T_c$) properties of a system but it is of limited value in estimating critical properties. Therefore, in our work, we did not attempt to do any calculation for critical exponents and related aspects of a phase transition. We compare the predictions of SCHA theory to numerical simulations on several $L\times L$ square lattices ($L=16,32,64,128$) using Monte Carlo and spin-dynamics (SD) simulations, which include effects due to all thermodynamically allowed excitations. We present the thermodynamic results in Sec. II, and in Sec. III, the calculation of the dynamical correlation function. The simulation procedures are discussed in Secs. II B and III B, and their comparison with the SCHA theoretical calculations is given in Sec. IV. Finally, our conclusions are given in Sec. V.

II. STATIC PROPERTIES

A. Self-consistent harmonic approximation

Since its original derivation by Bloch,[7] the self-consistent harmonic approximation has been found to account for the low temperature dependence of various properties of several magnetic insulators, which seem to be fairly well-described by the Heisenberg model.[8–10] Its usefulness stems mainly from the way it takes into account a substantial part of the interactions among spin waves, being characterized by simple temperature-dependent renormalization factors for the unperturbed spin wave energy.

We start by writing the spin components using the Dyson-Maleev representation of spin operators

$$S^x_{\mathbf{n}}=\frac{\sqrt{2S}}{2}(a_{\mathbf{n}}+a^\dagger_{\mathbf{n}})-\frac{1}{2\sqrt{8S}}(a^\dagger_{\mathbf{n}}a_{\mathbf{n}}a_{\mathbf{n}}+a^\dagger_{\mathbf{n}}a^\dagger_{\mathbf{n}}a_{\mathbf{n}}),$$

$$S^y_{\mathbf{n}}=\frac{\sqrt{2S}}{2i}(a_{\mathbf{n}}-a^\dagger_{\mathbf{n}})-\frac{1}{2i\sqrt{8S}}(a^\dagger_{\mathbf{n}}a_{\mathbf{n}}a_{\mathbf{n}}-a^\dagger_{\mathbf{n}}a^\dagger_{\mathbf{n}}a_{\mathbf{n}}), \qquad (2)$$

$$S^z_{\mathbf{n}}=S-a^\dagger_{\mathbf{n}}a_{\mathbf{n}},$$

where $a^\dagger_{\mathbf{n}}$ and $a_{\mathbf{n}}$ are the Bose spin operators on site $\mathbf{n}$. The harmonic spin wave Hamiltonian obtained from Eq. (1) is given by

$$H_0=\sum_{\mathbf{q}}\ \omega_{\mathbf{q}}a^\dagger_{\mathbf{q}}a_{\mathbf{q}}, \qquad (3)$$

where $a^\dagger_{\mathbf{q}}$ and $a_{\mathbf{q}}$ are the Fourier transforms of $a^\dagger_{\mathbf{n}}$ and $a_{\mathbf{n}}$, respectively, and

$$\omega_{\mathbf{q}}=4JS[1-\gamma(\mathbf{q})]+4KS, \qquad (4)$$

with $\gamma(\mathbf{q})=\frac{1}{2}[\cos q_x+\cos q_y]$. The spin wave approximation will be reasonable when $\langle a^\dagger_{\mathbf{n}}a_{\mathbf{n}}\rangle\ll S$, so it ought to be fairly good for anisotropies satisfying the relation $T\ll 4KS^2$.

Now we simplify the general model by reducing Hamiltonian (1) to an effective harmonic problem with the effect of anharmonicity embodied in temperature-dependent renormalized parameters. This means that the couplings of the model are replaced by quadratic interactions whose strength is then optimized. Details of this method may be found in the literature[7,9] and we give here only an outline of those steps pertinent to our present calculation.

We assume as effective Hamiltonian the appropriate form for a noninteracting gas of Bose excitations

$$\tilde{H}_0=\sum_{\mathbf{q}}\ E_{\mathbf{q}}a^\dagger_{\mathbf{q}}a_{\mathbf{q}}. \qquad (5)$$

The spin wave energy is obtained by a variational procedure based on the inequality for the free energy F

$$F\leqslant\tilde{F}_0+\langle H-\tilde{H}_0\rangle_0, \qquad (6)$$

where the brackets indicate the thermal average. Traces should be taken only over the physical states, that is, states with no more than $2S$ spin deviations on a single site. The minimization of Eq. (5) with respect to $E_{\mathbf{q}}$ determines the spin wave energies. We obtain, in the classical limit, following Rastelli *et al.*,[9]

$$E_{\mathbf{q}}(T)=4JS(1-\gamma(\mathbf{q}))[1-\tilde{\beta}(T)+\tilde{\eta}(T)]+4KS[1-\tilde{\beta}(T)-\gamma(\mathbf{q})\tilde{\eta}(T)], \qquad (7)$$

where

$$\tilde{\beta}(T)=\frac{T}{NS}\sum_{\mathbf{q}}\ \frac{1}{E_{\mathbf{q}}}, \qquad (8)$$

$$\tilde{\eta}(T)=\frac{T}{NS}\sum_{\mathbf{q}}\ \frac{\gamma(\mathbf{q})}{E_{\mathbf{q}}}, \qquad (9)$$

where N is the number of sites. Equations (7), (8), and (9) are coupled equations which we solved self-consistently by an iterative method. These coupled equations have a double-valued solution below T_c and no real solution above T_c: this is the typical behavior for self-consistent harmonic approximations and allows for easy determination of T_c. The lower branch (for $T<T_c$) has an unphysical temperature dependence and may be discarded as a spurious mathematical solution that is physically unstable. In Fig. 1 the spin wave energy for $K/J=0.05$ is given for two temperatures well below $T_c\approx 0.75J$: $T=0.3J$, and $T=0.6J$. The circles and stars shown in Fig. 1 were taken from our numerical simulation data (to be described in Sec. III B). As can be seen, the comparison between the SCHA and numerical results is remarkably good: the SCHA describes well the decrease of energy with increasing temperature (and, also, the energy dependence with the wave vector).

The reduced spontaneous magnetization along the z axis is given by

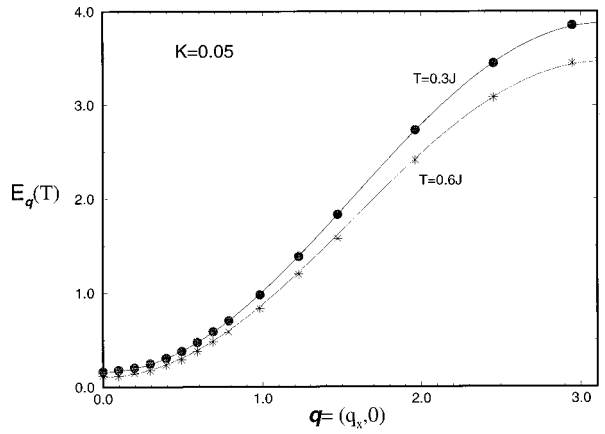

FIG. 1. The curves correspond to the spin wave energy [from Eq. (7)] for $T=0.3J$ (continuous), and $T=0.6J$ (dashed) for $K=0.05J$. The circles and stars correspond to the values extracted from our numerical simulations; error bars are smaller than the symbols.

$$\frac{M_z(T)}{M_z(0)}=1-\tilde{\beta}(T). \tag{10}$$

In Fig. 2, we present results obtained from Eq. (10) for $K/J=0.05$ and compare to our Monte Carlo (MC) data (obtained as described in Sec. II B). The slight overestimate of T_c from SCHA clearly is due to the fact that it does not include all possible modes of fluctuations, that are included in the MC calculations. The SCHA theory has no built-in requirement to make the magnetization null at the critical temperature T_c, and consequently, we find, as Fig. 2 shows, a nonzero value for $M_z(T_c)$. This is typical of SCHA approaches: the theory applies only below T_c, and for temperatures $T\geqslant T_c$ the magnetization is taken as zero, implying a discontinuous jump at T_c. In fact, the scaling of the MC data for $M_z(T)$ with system size L strongly suggests the presence of a discontinuous jump.

B. Monte Carlo

In order to evaluate the accuracy of the above theory, we calculated T_c and the magnetization and other thermodynamic quantities using a hybrid classical Monte Carlo approach on periodic $L\times L$ square lattices. We applied a combination of Metropolis single-spin moves and over-relaxation moves that modify all three spin components, and in addition, Wolff single-cluster operations[11] that modify *only* the S^z components. The over-relaxation and cluster moves are necessary to avoid critical slowing down near T_c, which is tending to freeze the S^z components. The single spin and over-relaxation moves are standard; here we give only a few details about the cluster algorithm. In the Wolff single-cluster algorithm, the cluster-flip operation we used only reverses the sign of S^z for all sites that have been included into the cluster. This is reminiscent of the Swendsen-Wang algorithm[12] for Ising models, but we only build one cluster at a time as in the Wolff algorithm. The cluster moves cannot be used alone because they do not change the *magnitudes* of S^z spin components.

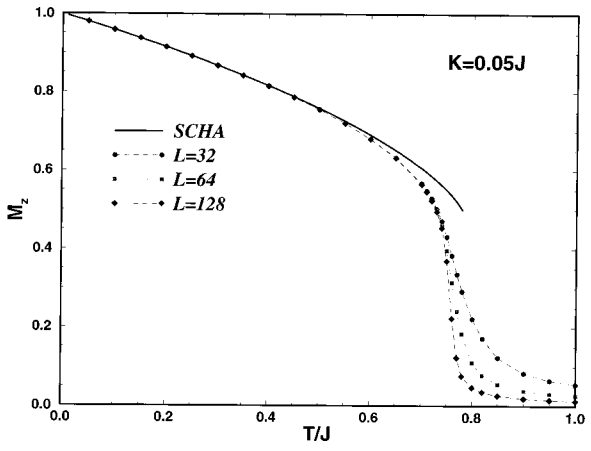

FIG. 2. Magnetization as a function of temperature for $K=0.05J$. Solid curve is the SCHA theory. Various symbols correspond to MC simulation for indicated system sizes; error bars are smaller than the symbols.

A cluster is built up starting from a randomly chosen seed site $\mathbf{n}$, immediately inverting its S^z component: $S^z_{\mathbf{n}}\rightarrow -S^z_{\mathbf{n}}$, and then including neighboring sites $\mathbf{n}+\mathbf{a}$ with a probability,

$$p_{\text{bond}}=\max[0,1-e^{-\beta\Delta E_{\mathbf{n},\mathbf{n}+\mathbf{a}}}]. \tag{11}$$

Here $\Delta E_{\mathbf{n},\mathbf{n}+\mathbf{a}}$ is the energy change involved if site $\mathbf{n}+\mathbf{a}$ is *not* flipped:

$$\Delta E_{\mathbf{n},\mathbf{n}+\mathbf{a}}=-2(J+K)S^z_{\mathbf{n}}S^z_{\mathbf{n}+\mathbf{a}}. \tag{12}$$

Note that in this formula site $\mathbf{n}$ was already included into the cluster and $S^z_{\mathbf{n}}$ was already inverted. Equation (11) represents the cluster growth as essentially a sequence of Metropolis decisions, according to whether $\Delta E_{\mathbf{n},\mathbf{n}+\mathbf{a}}$ is less than or greater than zero. Newly included sites then have their neighbors tested for inclusion until the cluster is done growing, at which point all included sites have already been modified.

We define one cluster sweep as building enough single clusters until the number of sites included into clusters is one quarter of the total number of sites in the system. Then we defined one hybrid Monte Carlo step as one over-relaxation sweep followed by one Metropolis single spin sweep followed by one Wolff cluster sweep. Equilibrium data shown here are averages over 10^5 to 4×10^5 Monte Carlo steps. The critical temperature was determined from the change in the distribution of z-component of total magnetization, which is easily characterized by Binder's fourth cumulant ratio,[13]

$$U_L=1-\frac{\langle M_z^4\rangle}{3\langle M_z^2\rangle^2}. \tag{13}$$

The crossing point of curves of $U_L(T)$ for different system sizes gives a good estimate of T_c. All calculations were made for square lattices of size $L\times L$, using unit spins $S=1$ and fixing $J=1$ while allowing K to be varied.

C. Static results

The critical temperature from the SCHA as a function of anisotropy parameter K/J is shown in Fig. 3 and compared with numerical MC estimates for a set of specific values of K/J ranging from 0.05 to 10.0. Generally, the SCHA overestimates T_c when compared to the MC results, because it does not fully take into account all possible fluctuations that are taking part in the transition. Notice that, as K increases,

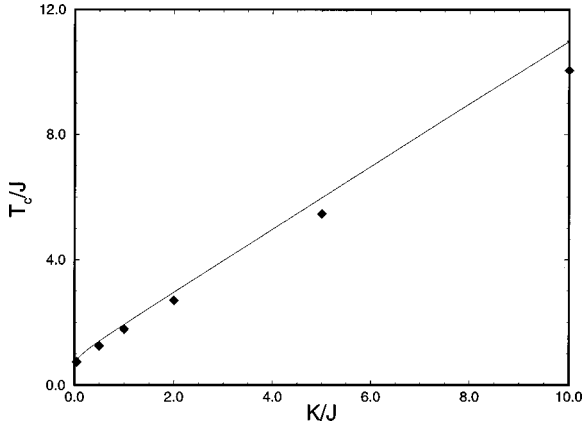

FIG. 3. Critical temperature as a function of the anisotropy parameter K/J. The symbols correspond to the values obtained in our MC calculation (as described in Sec. II B); error bars are smaller than the symbols.

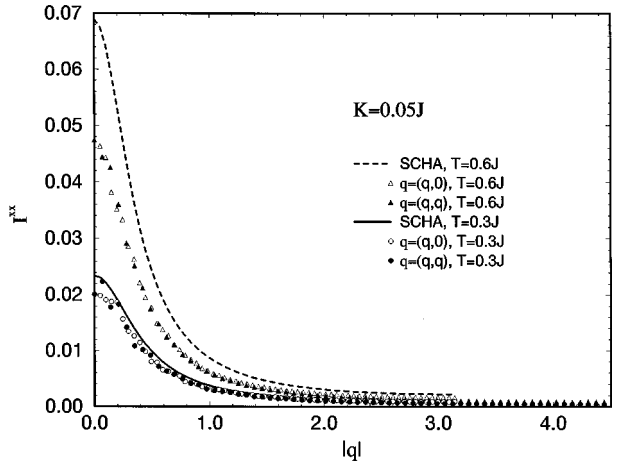

FIG. 4. In-plane integrated intensity I^{xx} versus wave vector, from SCHA (curves) compared with MC-SD (symbols) for $K=0.05J, L=128$.

the dependence of T_c on K/J becomes linear. For $K/J \gg 1$, we recover a continuous spin Ising Hamiltonian: Eq. (1) can be approximated as $H \approx J(1+K/J)S^z_{\mathbf{n}}S^z_{\mathbf{n}+\mathbf{a}} = \tilde{K}S^z_{\mathbf{n}}S^z_{\mathbf{n}+\mathbf{a}}$. Figure 3 shows that, for $K/J > 1.0$, the results follow a straight line with slope ≈ 1.0. We remark again that, strictly speaking, the analogy between Hamiltonian (1) and the continuous spin Ising model can only be expected to hold for $T \ll K$. For moderate and high temperatures, model (1) still exhibits the full entropy effects of a three-component spin model, resulting in a much lower transition temperature than a one-component Ising model. For this reason we cannot expect to compare our results to the ones obtained for the usual 2D Ising model.

Some of the drawbacks of the SCHA are well known: (i) it does not take into account strong coupling effects which are important at high temperatures and at short wavelengths; (ii) it also neglects the kinematical interaction and gives a first-order phase transition to the paramagnetic phase (where the true phase transition should be of second order). Notwithstanding this, we see that the theory gives results which compare quite well with the MC data we obtained.

This good agreement cannot be used to conclude that solitons do not have an important contribution to the properties of our model. As is well known, in the one dimensional easy-axis ferromagnet, the soliton connects two distinct ground states and has, therefore, a *global* effect in the system.[14] As a consequence, a pure spin wave calculation does not predict correctly all thermodynamic quantities. For instance, spin waves give a linear behavior with temperature T (for $T \to 0$) for the correlation length, while the soliton model predicts correctly an exponential behavior. In two dimensions, however, the soliton has only a *local* effect and its contribution to thermodynamic quantities should be small. The reasonable agreement of the SCHA calculation with the Monte Carlo data is not, per se, an indication that we should rule out topological effects. The signature of topological solitons is best analyzed in the dynamics where it should manifest as a central peak. This topic will be discussed in the following sections.

III. DYNAMIC CORRELATION FUNCTIONS

A. SCHA

From Hamiltonian (1) and using Eqs. (2), we obtain the time dependent correlation functions

$$\langle S^x_{\mathbf{q}}(t)S^x_{-\mathbf{q}}\rangle = \frac{S}{2}\langle [a_{\mathbf{q}}(t)+a^\dagger_{\mathbf{q}}(t)][a_{-\mathbf{q}}+a^\dagger_{-\mathbf{q}}]\rangle,$$

$$\langle S^y_{\mathbf{q}}(t)S^y_{-\mathbf{q}}\rangle = \frac{S}{2}\langle [a_{\mathbf{q}}(t)-a^\dagger_{\mathbf{q}}(t)][a_{-\mathbf{q}}-a^\dagger_{-\mathbf{q}}]\rangle,$$

$$\langle S^z_{\mathbf{q}}(t)S^z_{-\mathbf{q}}\rangle = \delta_{\mathbf{q},0}\langle S-(a^\dagger_l a_l)\rangle^2 + \langle \delta S^z_{\mathbf{q}}(t)\,\delta S^z_{-\mathbf{q}}\rangle, \quad (14)$$

where

$$\delta S^z_{\mathbf{q}}(t) = \frac{1}{N^{1/2}}\sum_{\mathbf{l}} e^{i\mathbf{q}\cdot\mathbf{l}}(a^\dagger_{\mathbf{l}}(t)a_{\mathbf{l}}(t) - \langle a^\dagger_{\mathbf{l}}(t)a_{\mathbf{l}}(t)\rangle). \quad (15)$$

The averages are readily evaluated, and give the xx- and yy-dynamical correlation functions:

$$\langle S^x_{\mathbf{q}}(t)S^x_{-\mathbf{q}}\rangle = \langle S^y_{\mathbf{q}}(t)S^y_{-\mathbf{q}}\rangle = \frac{S}{2}[n_{\mathbf{q}}e^{iE_{\mathbf{q}}t} + (n_{\mathbf{q}}+1)e^{-iE_{\mathbf{q}}t}], \quad (16)$$

where $n_{\mathbf{q}}$ is the Bose occupation number and $E_{\mathbf{q}}$ is the self-consistent spin wave frequency of Equation (5). Equation (16) leads to pure spin wave peaks for the spectral function:[15]

$$S^{xx}(\mathbf{q},\omega) = \frac{S}{2(2\pi)^2}[n_{\mathbf{q}}\delta(\omega - E_{\mathbf{q}}) + (n_{\mathbf{q}}+1)\,\delta(\omega+E_{\mathbf{q}})]. \quad (17)$$

The comparison between these SCHA results for S^{xx} and those obtained by spin dynamics simulation (Sec. III B) are shown in Figs. 1 and 4. These are discussed in more detail in Sec. IV B below.

The zz correlation contains, in addition to the Bragg scattering at $\mathbf{q}=\mathbf{0}$, a term describing correlations in the fluctuations of the spin's z component. Evaluating the averages, we obtain

$$\langle \delta S^z_{\mathbf{q}}(t)\,\delta S^z_{-\mathbf{q}}\rangle = \frac{1}{2N}\sum_{\mathbf{k}} [e^{i\Omega t}(1+n_{\mathbf{q}/2-\mathbf{k}})n_{\mathbf{q}/2+\mathbf{k}} + e^{-i\Omega t}(1+n_{\mathbf{q}/2+\mathbf{k}})n_{\mathbf{q}/2-\mathbf{k}}], \tag{18}$$

where

$$\Omega = E_{\mathbf{q}/2+\mathbf{k}} - E_{\mathbf{q}/2-\mathbf{k}}. \tag{19}$$

Equation (18) corresponds to the various two-spin-wave scattering terms. It is interesting to notice that, to this order, only *difference* processes contribute to the dynamics. The time Fourier transform of Eq. (18), together with the thermodynamic limit $L\to\infty$, gives us the response function[15]

$$S^{zz}(\mathbf{q},\omega) = \frac{1}{2(2\pi)^4}\int d\mathbf{k}[n_{\mathbf{q}/2+\mathbf{k}}(1+n_{\mathbf{q}/2-\mathbf{k}})\,\delta(\omega-\Omega) + n_{\mathbf{q}/2-\mathbf{k}}(1+n_{\mathbf{q}/2+\mathbf{k}})\,\delta(\omega+\Omega)]. \tag{20}$$

Using the delta functions we obtain integrals on the contours $\mathcal{C}^{\pm}$ defined by $\omega=\pm\Omega$: the first integral is

$$\frac{1}{2(2\pi)^4}\int_{\mathcal{C}^+} dl_{\mathbf{k}} n_{\mathbf{q}/2+\mathbf{k}}(1+n_{\mathbf{q}/2-\mathbf{k}})|\nabla_k\Omega|^{-1}, \tag{21}$$

where $dl_{\mathbf{k}}$ is the contour element and $|\nabla_k\Omega|$ designates the Jacobian of the involved transformation. There is a singularity in these integrands for every minimum or maximum of Ω and the spectrum is in general quite complicated. We emphasize that, here, we have also used the self-consistent result obtained in Sec. II for the spin wave energies. Results for the spectral functions obtained from Eq. (20) will be compared with those from MC-SD simulations below in Sec. IV.

B. Spin dynamics simulations

The spin dynamics simulation is standard.[16–18] Here we summarize the method and describe the particular numerical parameters used. For a given temperature, a set of 200 initial states was taken from the Monte Carlo simulation to serve as initial conditions for the spin-dynamics time integration. The nonlinear equations of motion associated with Hamiltonian (1) are

$$\frac{d\mathbf{S_n}}{dt} = \mathbf{S_n}\times\left[\tilde{J}\sum_{\mathbf{a}}\mathbf{S_{n+a}}\right], \tag{22}$$

where $\tilde{J}$ is the diagonal matrix of exchange couplings,

$$\tilde{J} = \begin{pmatrix} J & 0 & 0 \\ 0 & J & 0 \\ 0 & 0 & J+K \end{pmatrix}. \tag{23}$$

These were integrated forward in time using a standard fourth order Runge-Kutta scheme with time step $h=0.035/J$ (for small K/J). By saving data for time Fourier transforms at intervals $dt=6h$, allows for measuring $S(\mathbf{q},\omega)$ out to $\omega_{\max}=2\pi/dt\approx 30J$. We saved a total of $N_t=2^{11}$ samples in time, integrating out to final time $t_{\max}=N_t dt \approx 430/J$, giving a frequency resolution of $\delta\omega=2\pi/t_{\max}\approx 0.015J$. The space and time Fourier-transformed spin-spin correlations were averaged over the 200 initial states to get $S(\mathbf{q},\omega)$, for both in-plane and out-of-plane spin components.

IV. DYNAMIC CORRELATIONS: RESULTS

A. Small lattices ($L\leqslant 64$)

At low temperatures $T\ll T_c$, we especially expect that the SCHA should give good agreement with the spin-dynamics simulation. We had noticed, however, that spin dynamics for small lattices gives an interesting set of unevenly spaced peaks in $S^{zz}(\mathbf{q},\omega)$, in contrast to one sharp peak at the spin wave frequency in $S^{xx}(\mathbf{q},\omega)$, and also in contrast to the smooth behavior predicted for $S^{zz}(\mathbf{q},\omega)$ by Eq. (20). Also, an intensity *maximum* in $S^{zz}(\mathbf{q},\omega)$ for $\omega\to 0$ is present for wave vectors of the form $\mathbf{q}=(2\pi/L)(2m,0)$, where m is an integer. On the other hand, for wave vectors $\mathbf{q}=(2\pi/L)(2m+1,0)$, there is an intensity *minimum* in $S^{zz}(\mathbf{q},\omega)$ at $\omega\to 0$. In order to see if the SCHA theory could explain this interesting result we restarted our calculation from Eq. (18), restricting the sums to the discrete wave vectors $\mathbf{k}=(2\pi/L)(m,n)$ of each lattice. Also, the time integration for $S(\mathbf{q},\omega)$ was performed for a *finite* time interval $t_{\max}$,

$$S^{zz}(\mathbf{q},\omega) = \frac{1}{2\pi}\int_{-t_{\max}/2}^{t_{\max}/2} S^{zz}(\mathbf{q},t)e^{-i\omega t}\,dt, \tag{24}$$

where $t_{\max}$ was taken to be the same as the integration time $(430/J)$ used in our simulations. Equation (18) is modified for a finite time interval, and a complete analysis leads to

$$S^{zz}(\mathbf{q},\omega) = \frac{t_{\max}}{2N(2\pi)^3}\sum_{\mathbf{k}}\left\{ n_{\mathbf{q}/2+\mathbf{k}}(1+n_{\mathbf{q}/2-\mathbf{k}}) \times\left[\frac{\sin[(\omega-\Omega)t_{\max}/2]}{(\omega-\Omega)t_{\max}/2}\right]^2 + n_{\mathbf{q}/2-\mathbf{k}}(1+n_{\mathbf{q}/2+\mathbf{k}}) \times\left[\frac{\sin[(\omega+\Omega)t_{\max}/2]}{(\omega+\Omega)t_{\max}/2}\right]^2\right\}. \tag{25}$$

The expression can be thought to represent $S(\mathbf{q},\omega)$ as a sum over a set of narrow peaks of width approximately $2/t_{\max}$, centered at frequencies Ω, determined by choosing $\mathbf{k}$ such that both $\mathbf{q}/2+\mathbf{k}$ and $\mathbf{q}/2-\mathbf{k}$ in Eq. (19) are allowed discrete wave vectors. Besides restricting the sum in Eq. (25) to the discrete set of lattice wave vectors, the finite time integration $t_{\max}$ implies discrete frequency increments $\delta\omega=2\pi/t_{\max}\approx 0.015J$, the same as in our spin dynamics simulation.

Examination of Eqs. (19) and (25) allows us to conclude that a nonzero intensity in $S^{zz}(\mathbf{q},\omega\to 0)$ can exist for *all* wave vectors and not only for those of the form $\mathbf{q}=(2\pi/L)(2m,0)$. However, a little consideration shows that if $\mathbf{q}/2$ does not fall on a reciprocal lattice vector, then it is impossible to choose a value of $\mathbf{k}$ in Eq. (19) to give $\Omega=0$. Therefore, for wave vectors $\mathbf{q}=(2\pi/L)(2m+1,0)$, none of the multiple peaks in Eq. (25) will be centered at zero frequency, and $S^{zz}(\mathbf{q},\omega\to 0)$ is a local minimum. Although no peak is centered at zero, the tails can contribute

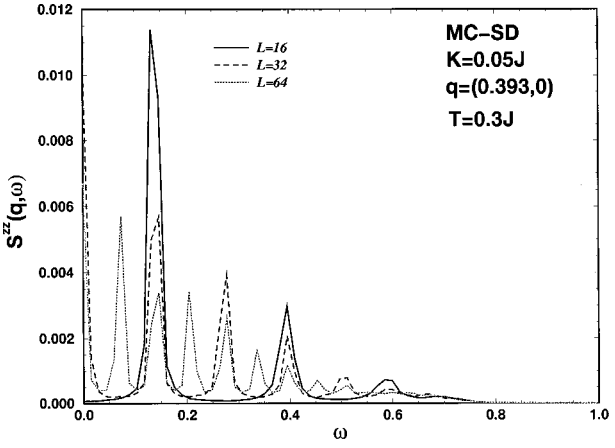

FIG. 5. $S^{zz}(\mathbf{q},\omega)$ obtained from numerical simulation for $K=0.05J$, $T=0.3J$, and $L=16,32,64$, and wave vector $\mathbf{q}=(0.393,0)$.

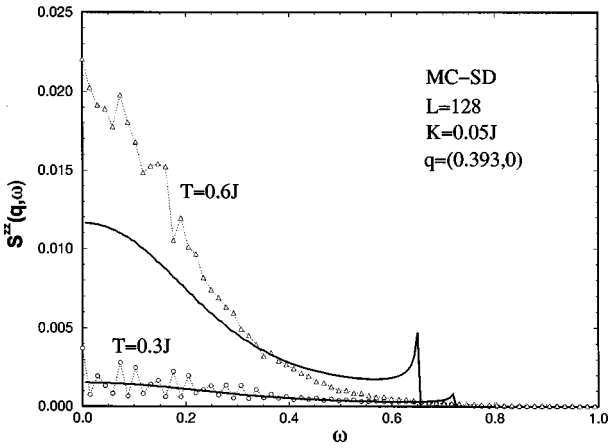

FIG. 7. $S^{zz}(\mathbf{q},\omega)$ from (continuous line) continuum limit (20) and from (circles and triangles) numerical simulation for $K=0.05J$, $T=0.3J$, and $T=0.6J$, and wave vector $\mathbf{q}=(0.393,0)$.

there. On the other hand, for wave vectors such as $\mathbf{q}=(2\pi/L)(2m,0)$, and $\mathbf{q}=(2\pi/L)(m,m)$, we see that $\mathbf{q}/2$ falls on a highly symmetric point in the reciprocal lattice, and it is always possible to choose $\mathbf{k}$ to get $\Omega=0$ in Eq. (19). Then for these cases, there is a peak at zero frequency, and $S^{zz}(\mathbf{q},\omega\rightarrow 0)$ is a local maximum.

The overall behavior of $S^{zz}(\mathbf{q},\omega)$ with the lattice size obtained either by numerical simulation (Fig. 5) or by the calculation of Eq. (25) (Fig. 6) agree very well. In order to make this comparison, because the spin-dynamics simulations are purely classical, it is necessary to replace all factors of $(1+n_{\mathbf{q}})$ in the SCHA expressions by $n_{\mathbf{q}}$. Also, these occupation numbers were evaluated by their classical limit, $n_{\mathbf{q}}=T/E_{\mathbf{q}}$, consistently with the static calculations in Sec. II. Figures 5 and 6 were obtained for $K/J=0.05$ (where $T_c\approx 0.75J$), $\mathbf{q}=(0.393,0)$, and $T=0.3J$ for lattice sizes $L=16$, 32, and 64.

Comparing the several peaks shown in Figs. 5 and 6, for a specific value of L, we see that they are positioned around the same frequencies. The important feature is that as the system size is increased, the spacing between the multiple peaks in $S^{zz}(\mathbf{q},\omega)$ becomes smaller as $1/L$. In addition, for a longer time integration $t_{\max}$, the widths of the peaks will be narrower, and therefore they will become more distinct. As far as we are aware, this strong finite-size effect in low-temperature spin-dynamics simulations is a feature that has been previously ignored. It is very likely, however, that it appears in any related models. For example, finite-size effects most likely explain similar low-temperature multiple-peak features that have appeared in $S(\mathbf{q},\omega)$ calculated for the 2D Heisenberg model with easy-plane anisotropy.[18,19]

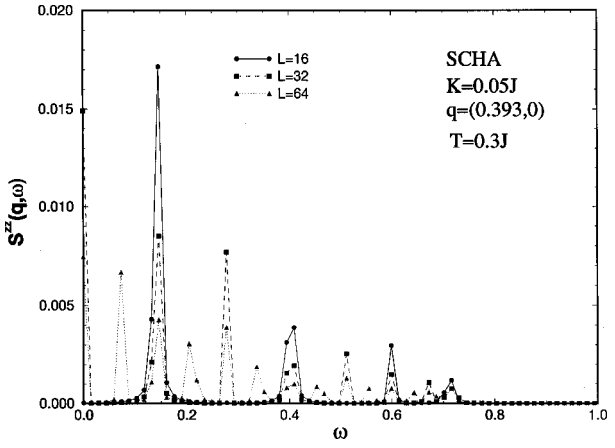

FIG. 6. $S^{zz}(\mathbf{q},\omega)$ obtained from discrete summation (25) for $K=0.05J$, $T=0.3J$, and $L=16,32,64$, and wave vector $\mathbf{q}=(0.393,0)$.

B. Large lattices ($L\geqslant 128$)

The SCHA calculation [Eq. (17)] and the MC-SD simulations both give single narrow spin wave peaks in $S^{xx}(\mathbf{q},\omega)$, regardless of lattice size. The MC-SD peak positions for $L=128$ have been compared with the SCHA results in Fig. 1, and agree very well for the temperatures studied. The SCHA theory gives peaks of zero width, thus it makes sense to compare the integrated intensities for the positive frequency peak, $I^{xx}=\int_0^{+\infty} dw\, S^{xx}(\mathbf{q},\omega)$. These are shown in Fig. 4, where the MC-SD results are compared to those obtained from Eq. (17), $I^{xx}=Sn_{\mathbf{q}}/(8\pi^2)$. For the lower temperature, $T=0.3J$, there is very good agreement. The good low-T agreement, with no adjusted parameters, shows that the approximations made in the SCHA theory are reasonable where we expect this simple theory to work. For $T=0.6J$, however, the MC-SD result is suppressed compared to the SCHA prediction. Currently we cannot say whether this suppression should be better described by spin wave interaction terms or possibly by nonlinear excitations such as solitons or domain walls. Clearly, both effects could become more important as the critical temperature is approached.

For $S^{zz}(\mathbf{q},\omega)$, the widths of the multiple peaks are determined both by the intrinsic width due to temperature, and the width $2\pi/t_{\max}$ inherent in the spin-dynamics simulation. For larger lattices, or higher temperatures, the spacing of the multiple peaks in $S^{zz}(\mathbf{q},\omega)$ becomes smaller than their measured widths, the peaks merge and the curve is much smoother. Thus in our simulations the finite-size effects are quite well smoothed out for lattices $L>128$ and/or for high temperatures. In Figs. 7–10, for $K=0.05J$, several $\mathbf{q}$ values,

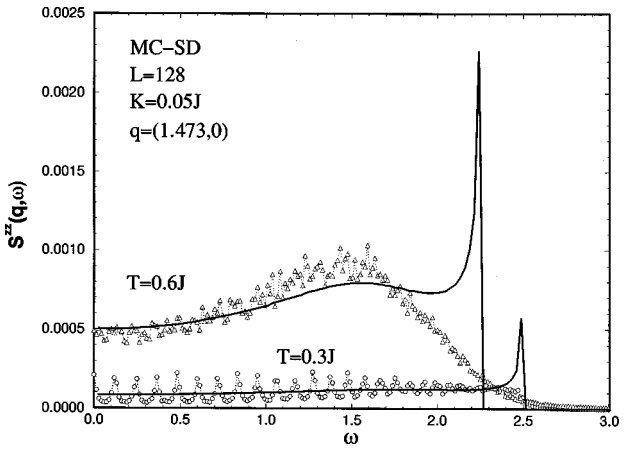

FIG. 8. $S^{zz}(\mathbf{q},\omega)$ from (continuous line) continuum limit (20) and from (circles and triangles) numerical simulation for $K=0.05J, T=0.3J$, and $T=0.6J$, and wave vector $\mathbf{q}=(1.473,0)$.

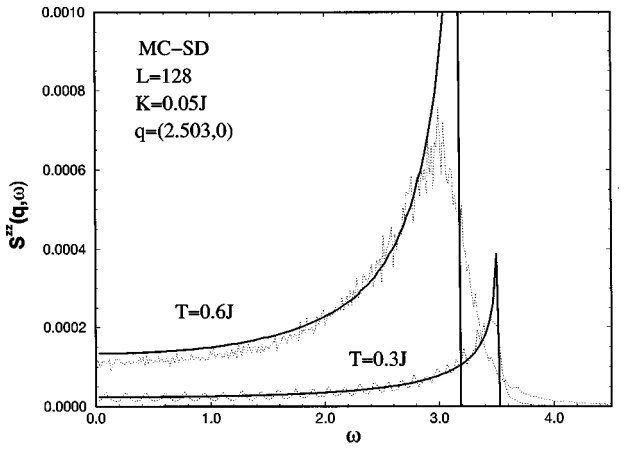

FIG. 9. $S^{zz}(\mathbf{q},\omega)$ obtained from (continuous line) continuum limit (20) and from (circles and triangles) numerical simulation for $K=0.05J$, $T=0.3J$, and $T=0.6J$, and wave vector $\mathbf{q}=(2.503,0)$.

and $L=128$ we see that the simulation data for the higher temperature $T=0.6J$ are smooth while the data for $T=0.3J$ still show sharp peaks.

Using the ''discrete'' equation (25) for obtaining $S^{zz}(\mathbf{q},\omega)$ for lattice size $L=128$ we do not get rid of the multiple peak structure even for $T=0.6J$. This can be seen in Fig. 11 where the three types of calculations — numerical simulation, discrete summation (25) and continuum limit (20) — we used to obtain $S^{zz}(\mathbf{q},\omega)$ are shown for $K=0.05$, $T=0.6J$, and $\mathbf{q}=(\mathbf{1.03},0)$. Typically, the discrete SCHA summation results in an $S^{zz}(\mathbf{q},\omega)$ curve with very strong multiple peak structure. In order to smooth out the structure obtained from Eq. (25) it is necessary to consider much larger lattices ($L>500$). It is natural to expect that it is more difficult to smooth out the spectra obtained by Eq. (25) than the one obtained via spin dynamic simulation. Clearly the MC-SD calculation contains more fluctuations and therefore greater peak widths, especially as T approaches T_c, whereas in expression (25) all spin wave peaks have very narrow widths determined only by the integration time. Instead of trying to smooth the SCHA spectra by considering larger and larger lattices for the calculation of Eq. (25)— which requires extra computational effort — we can go to the continuum approximation limit built in Eq. (20). In fact, most real systems contain a large number N of spins ($N\rightarrow\infty$) and effects due to the discreteness of the lattice are not important. These macroscopic systems will be better represented by the continuous approximation built in Eq. (20). Figures 7–10 show the spectral functions obtained by numerically evaluating Eq. (20) for $K=0.05$, $T=0.3J$, and $T=0.6J$, for the following wave vectors: $\mathbf{q}=(0.393,0)$, $(1.473,0)$, $(2.50,0)$ and $(1.03,1.03)$. These are compared with the corresponding MC-SD calculations for 128×128 lattices.

Obviously, considering the dynamical simulation, it is not possible to go to the $N\rightarrow\infty$ limit: the computational cost in simulations increases tremendously with N. Nevertheless, we can remark on interesting features concerning the results obtained from the SCHA calculation and from numerical simulation procedures. First, the ''cutoff frequency'' or upper frequency limit below which $S^{zz}(\mathbf{q},\omega)$ has appreciable intensity does not depend on the lattice size and on the kind of calculation performed to obtain $S^{zz}(\mathbf{q},\omega)$. This can be observed in Figs. 5, 6, and 7, which correspond to the three different ways we have used to obtain the spectral function for different lattice sizes but for the same wave vector $\mathbf{q}=(0.393,0)$.

In Fig. 12 we show the comparison of the cutoff frequency $\Delta\omega$ of the obtained spectral functions in the whole $|\mathbf{q}|$ range for wave vectors like $\mathbf{q}=(q,0)$: the data were obtained for $K=0.05J$ and $T=0.3J$. The comparison is remarkably good (a similar agreement is obtained for $T=0.6J$). We see that, for small $|\mathbf{q}|$, the frequency limit $\Delta\omega$ increases linearly with the wave vector. A trivial analysis of Eq. (20) leads us to the conclusion that $\Delta\omega$ must be related to the maximum value Ω can have for each $\mathbf{q}$. From Eq. (19) we easily obtain that $\Omega_{\max}=B(T)\sin|q|/2$ where $B(T)=\epsilon JS[1-\beta(T)+\eta(T)(1+K)]$ and $\epsilon=1$ for $\mathbf{q}=(q,0)$ wave vectors and $\epsilon=2$ for $\mathbf{q}=(q_x,q_x)$. For comparison, we show in Fig. 12 a curve (dashed line) corresponding to $\Omega_{\max}$.

Second, the SCHA curves corresponding to wave vectors of the form $\mathbf{q}=(q,0)$ or $(0,q)$ (Figs. 7–9) show a sharp peak

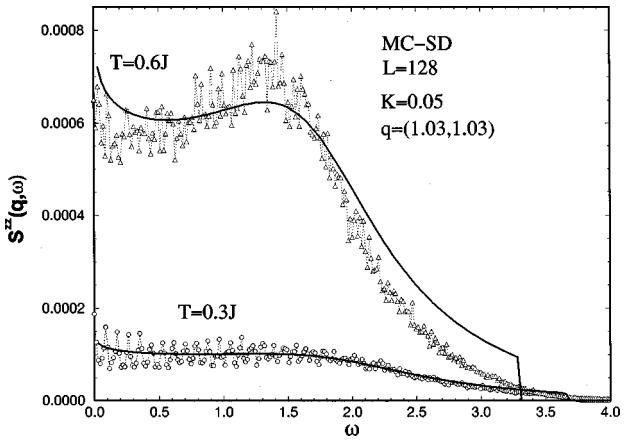

FIG. 10. $S^{zz}(\mathbf{q},\omega)$ obtained from (continuous line) continuum limit (20) and from (circles and triangles) numerical simulation for $K=0.05J$, $T=0.3J$, and $T=0.6J$, and wave vector $\mathbf{q}=(1.03,1.03)$.

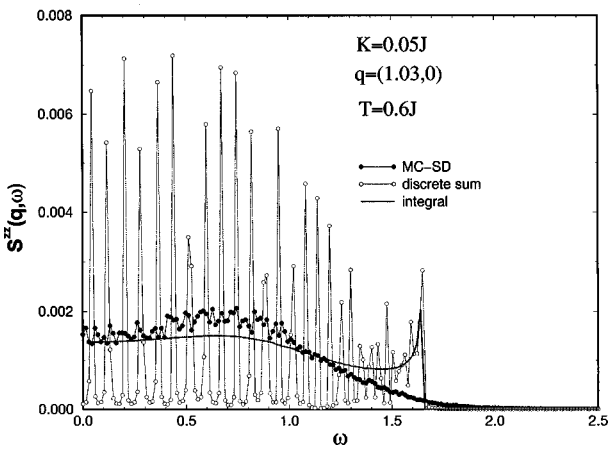

FIG. 11. $S^{zz}(\mathbf{q},\omega)$ obtained from numerical simulation (filled circles), discrete summation (empty circles) and from continuum limit (line) for $K=0.05J$, $T=0.6J$, $L=128$, and wave vector $\mathbf{q}=(1.03,0)$.

at higher frequencies, just before the spectral function vanishes. For wave vectors like $\mathbf{q}=(q,q)$, this sharp peak is only observed near the point (π,π), and not for smaller $|\mathbf{q}|$, as can be seen in Fig. 10. The appearance or not of these peaks in the SCHA calculation depends on the behavior of the density of states $|\nabla\Omega|^{-1}$ in Eq. (21). Figures 13 and 14 show contours of $\Omega(\mathbf{q},\mathbf{k})$ in the $\mathbf{k}$-plane, for $\mathbf{q}=(0,0.393)$ and $\mathbf{q}=(1.03,1.03)$, respectively, for $T=0.3J$. For $\mathbf{q}$ in the (10) or (01) directions, the contours are straight lines (Fig. 13). They become very widely spaced near $k_x=\pi/2$, or near $k_x=\pi/2$, where Ω approaches $\Omega_{\max}$, and $|\nabla\Omega|^{-1}$ becomes very large along the whole straight contour. The integration along the contour in Eq. (21) then leads to the sharp peaks at $\omega\rightarrow\Omega_{\max}$ seen in $S^{zz}(\mathbf{q},\omega)$. For $\mathbf{q}$ along the (11) direction, the contours are curves (Fig. 14). For moderate values of $|\mathbf{q}|$, the higher contours (near $\Omega_{\max}$) approximate small circles, having limited total length and thus creating no sharp peak in $S^{zz}(\mathbf{q},\omega)$. Only for $\mathbf{q}$ very close to the point (π,π) is the effect due to the divergence of $|\nabla\Omega|^{-1}$ more important than the contour length, and there a sharp peak at $\omega\rightarrow\Omega_{\max}$ does occur.

It is interesting to notice that this peak is also present in the data obtained from the discrete spin wave calculation

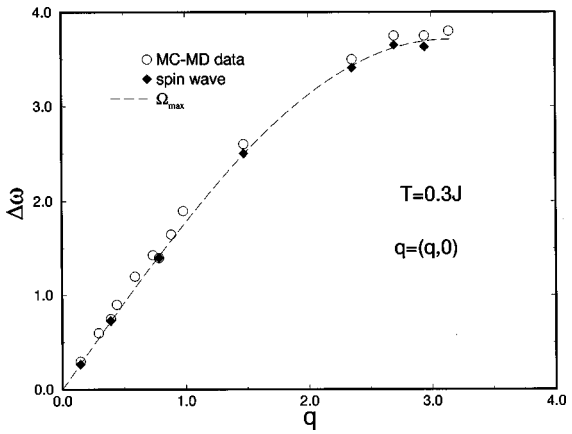

FIG. 12. Cutoff frequency of $S^{zz}(\mathbf{q},\omega)$ as a function of q for $K=0.05J$ and $T=0.3J$.

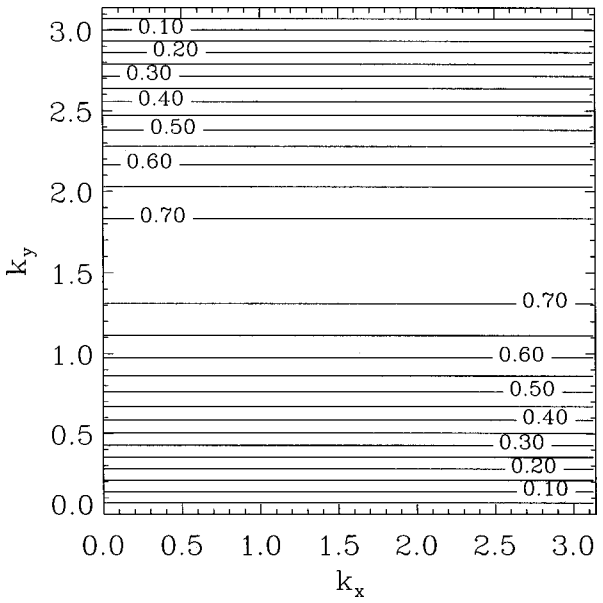

FIG. 13. Contours of difference frequency $\Omega(\mathbf{q},\mathbf{k})$ for $T=0.3J$ and $\mathbf{q}=(0,0.393)$ as functions of $\mathbf{k}$.

(Fig. 11) although the density of states does not appear explicitly in Eq. (25). Nevertheless, the two spin wave calculations must, in fact, give similar results because Eqs. (20) or (21) correspond to the $t_{\max}\rightarrow\infty$, and $N\rightarrow\infty$ limits of Eqs. (25). For small wave vectors, this sharp high frequency peak is not seen in the simulation data suggesting that inclusion of higher order terms in the spin wave theory would probably lead to the attenuation of this peak in the SCHA results. As the wave vector $|\mathbf{q}|$ increases, a lateral shoulder develops in the spectra obtained from both numerical simulation and SCHA calculations; it is already well defined for $q\sim0.50$. For very large wave vectors, as in Fig. 9, the lateral shoulder for the MC-SD data occurs in the frequency region affected by the increase of $|\nabla\Omega|^{-1}$. This shoulder seems to be a

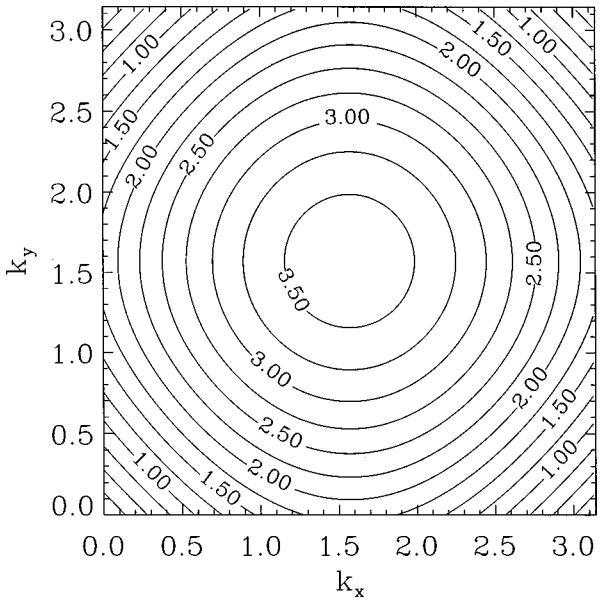

FIG. 14. Contours of difference frequency $\Omega(\mathbf{q},\mathbf{k})$ for $T=0.3J$ and $\mathbf{q}=(1.03,1.03)$ as functions of $\mathbf{k}$.

characteristic of two-spin-wave processes because it has been observed in other systems.[20]

As the temperature increases, the width of the spectral function $S^{zz}(\mathbf{q},\omega)$ decreases but its height increases. The spin wave calculation seems to agree well with the MC-SD data for large wave vectors, even for $T=0.6J$. For small wave vectors and higher temperature, however, $S^{zz}(\mathbf{q},\omega)$ from the SCHA calculation is smaller than the MC-SD data (Fig. 7), suggesting that at high temperatures other processes could be contributing to the dynamical properties of this system. For systems with easy-axis anisotropy one can expect the formation of domains, as in the two-dimensional Ising model, and, also, localized solitons.[21] In particular, it is usually expected[22] that localized solitons would contribute to the dynamical correlation function in the $\omega\rightarrow 0$ (central peak) region and, mostly, for small wave vectors.

V. CONCLUSIONS

We have applied a self-consistent harmonic approximation to the easy-axis model, obtaining the spin wave energies, critical temperature and dynamic correlation functions. We also demonstrated how it is possible to apply the Wolff cluster Monte Carlo scheme to this easy-axis model, by having it act on only the S^z spin components. For the critical temperature, the SCHA and MC results agree favorably over a wide range of easy-axis anisotropy, both giving T_c increasing linearly with K for $K\gg J$. The spin-dynamics calculation of dynamic correlation functions shows interesting multiple-peak features in $S^{zz}(\mathbf{q},\omega)$, that are most easily seen in small lattices. These finite-size dynamical features are correctly described by the SCHA, especially for T far below T_c. Similar features should appear in models with other symmetries: there are strong evidences that these effects were also observed in other simulations of two dimensional easy-plane models.[18]

All the dynamical calculations discussed in this work were performed for anisotropy parameter $K=0.05$, which corresponds to a transition temperature $T_c=0.75J$. For this anisotropy, two temperatures were analyzed: $T=0.3J\ll T_c$, and $T=0.6J$. We could not expect that the spin wave calculation performed here, which neglects higher order terms in the spin interactions, would reproduce exactly the simulation data. However, the agreement for the lowest temperature, $T=0.3J$, is very good. It is also surprisingly good for $T=0.6J$, a relatively high temperature, and large wave vectors where a lateral peak is seen to develop. At $T=0.6J$, for small wave vectors and small frequencies, the SCHA function for S^{zz} shows a central peak with height *smaller* than the one obtained from MC-SD simulation. On the other hand, the SCHA prediction for the integrated intensity I^{xx} for the *in-plane* correlations lies *above* the MC-SD data for $T=0.6J$. These features may suggest that other excitations, like localized solitons and domain walls, may contribute to the dynamical correlation function as the temperature approaches the critical temperature. It was shown[5] that the density of these localized solitons increases exponentially with T as $T\rightarrow T_c$ and, then, one should expect that their contribution to the dynamics of the system becomes more important for temperatures $T\sim T_c$. To stress this conclusion, we remark that $S^{xx}(\mathbf{q},\omega)$ obtained by MC-SD simulation for $T>T_c$ (not shown here because SCHA cannot be compared in this temperature regime) does show a central peak ($\omega\sim 0$) that increases with T. Its properties will be analyzed in a future work.

We conclude by saying that the two-spin wave calculation can explain the main features obtained from Monte Carlo spin-dynamics simulation at very low temperatures. As $T\rightarrow T_c$, the comparison between SCHA spin-wave calculation and the numerical simulation data suggests that other excitations may contribute to the dynamic properties of the model. However, a better understanding concerning the contributions these excitations might give to the dynamic spectral functions requires some theory which takes into account the existence of such objects. To our knowledge, such a theory for easy-axis anisotropy two-dimensional systems is not available in the literature.

ACKNOWLEDGMENTS

The authors gratefully acknowledge the support of NSF DMR-9412300, NSF INT-9502781, NSF CDA-9724289, FAPEMIG, CAPES-DAAD, and CNPq.

*Permanent address: Department of Physics, Kansas State University, Manhattan, KS 66506-2601. Electronic address: wysin@phys.ksu.edu

†Permanent address: Department of Physics, University of Bayreuth, Bayreuth, Germany.

[1] *Low Dimensional Conductors and Superconductors*, Vol. 155 of *NATO Advanced Study, Institute, Series B: Physics*, edited by D. Jerome and L. G. Caron (Plenum, New York, 1987).

[2] J.M. Kosterlitz and D.J. Thouless, J. Phys. C **6**, 1181 (1973); V.L. Berezinskii, Zh. Eksp. Teor. Fiz. **59**, 97 (1970) [Sov. Phys. JETP **32**, 493 (1970)].

[3] *Magnetic Properties of Layered Transition Metal Compounds*, edited by L.J. de Jongh (Kluwer, Dordrecht, 1989).

[4] B.A. Ivanov and A.K. Kolezhuk, Low Temp. Phys. **21**, 275 (1995).

[5] B.V. Costa, M.E. Gouvêa, and A.S.T. Pires, Phys. Rev. B **50**, 3828 (1994).

[6] R.H. Hobart, Proc. Phys. Soc. London **82**, 201 (1963); G.H. Derrick, J. Math. Phys. **5**, 1252 (1964).

[7] M. Bloch, J. Appl. Phys. **34**, 1151 (1963).

[8] P.D. Loly, J. Phys. C **4**, 1365 (1971).

[9] E. Rastelli, A. Tassi, and L. Reatto, J. Phys. C **7**, 1735 (1974).

[10] D.A. Poling and R.H. Parmenter, Phys. Rev. B **16**, 3240 (1977).

[11] U. Wolff, Nucl. Phys. **B300**, 501 (1988); Phys. Rev. Lett. **62**, 361 (1989).

[12] R.H. Swendsen and J.-S. Wang, Phys. Rev. Lett. **58**, 86 (1987).

[13] See *Finite Size Scaling and Numerical Simulation of Statistical Systems*, edited by V. Privman (World Scientific, Singapore, 1990).

[14] M.E. Gouvêa and A.S.T. Pires, Phys. Lett. **114A**, 503 (1986).

[15] In going over from the discrete weights defined at discrete wave vectors and labeled by subscripts **q**, to the related continuum densities such as $S^{zz}(q,w)$, a factor of $1/(2\pi)$ appears for each space or time dimension. Also, the discrete summations over **k**

have been replaced by the usual prescription, in 2D, $\Sigma_{\mathbf{k}} \rightarrow N/(2\pi)^2 \int d\mathbf{k}$.

[16] C. Kawabata, M. Takeuchi, and A.R. Bishop, J. Magn. Magn. Mater. **54-57**, 871 (1986); J. Stat. Phys. **43**, 869 (1986).

[17] G.M. Wysin and A.R. Bishop, Phys. Rev. B **42**, 810 (1990).

[18] H. G. Evertz and D.P. Landau, Phys. Rev. B **54**, 12 302 (1996).

[19] M.E. Gouvêa and G.M. Wysin, Phys. Rev. B **56**, 14 192 (1997).

[20] M.E. Gouvêa and A.S.T. Pires, J. Phys. C **20**, 2431 (1987).

[21] A.M. Kosevich, B. Ivanov, and A. Kovalev, Physics Rep. **194**, 117 (1990).

[22] F.G. Mertens, A.R. Bishop, G.M. Wysin, and C. Kawabata, Phys. Rev. B **39**, 591 (1989).